Observational constraint from the heaviest pulsar PSR J0952-0607 on the equation of state of dense matter in relativistic mean field model

Raj Kumar,[1,*] Mukul Kumar,[1] Virender Thakur,[1,†] Sunil Kumar,[1] Pankaj Kumar,[2] Anuj Sharma,[1] B. K. Agrawal,[3,‡] and Shashi K. Dhiman[1,4,§]

[1]*Department of Physics, Himachal Pradesh University, Shimla-171005, India*
[2]*Department of Applied Sciences, CGC College of Engineering, Landran, Mohali-140307, India*
[3]*Saha Institute of Nuclear Physics, 1/AF Bidhannagar, Kolkata-700064, India*
[4]*School of Applied Sciences, Himachal Pradesh Technical University, Hamirpur-177001, India*

(Received 7 January 2023; revised 6 April 2023; accepted 4 May 2023; published 30 May 2023)

In the present work, we constrain the equation of state of dense matter in the context of heaviest observed neutron-star mass $M_{\max} = (2.35 \pm 0.17)M_{\odot}$ for the black widow pulsar PSR J0952-0607. We propose three interactions HPU1, HPU2 and HPU3 (named after Himachal Pradesh University) for the relativistic mean-field model, which include different combinations of nonlinear, self-couplings, and cross couplings among isoscalar-scalar σ, and isoscalar-vector ω and isovector-vector ρ meson fields up to the quartic order. These interactions are in harmony with the finite nuclei and bulk nuclear matter properties. The equations of state computed by using newly generated interactions for the β-equilibrated nucleonic matter satisfy the heaviest observed neutron-star mass $M_{\max} = (2.35 \pm 0.17)M_{\odot}$ for the black widow pulsar PSR J0952-0607. The results for the radius $R_{1.4}$ and dimensionless tidal deformability $\Lambda_{1.4}$ corresponding to the canonical mass are also presented and agree well with the GW170817 event and astrophysical observations. The radius of $2.08M_{\odot}$ neutron-star mass is predicted to be in the range $R_{2.08} = 12.98$–13.09 km which also satisfy the NICER observations by Miller *et al.* [Astrophys. J. Lett. **918**, L28 (2021)] and Riley *et al.* [Astrophys. J. Lett. **918**, L27 (2021)]. A covariance analysis is also performed to assess the theoretical uncertainties of model parameters and to determine their correlations with nuclear matter observables.

DOI: 10.1103/PhysRevC.107.055805

I. INTRODUCTION

Neutron stars are stellar objects made of highly dense asymmetric matter and have extreme properties. The dense core of the neutron star enables us to study nuclear matter beyond saturation density. The composition of the matter at such high density is not known exactly to the date, but the thermodynamic state of the matter is theorized by the equation of state (EoS). In recent years, many advances in astrophysical experiments have probed new constraints on EoS by studying properties like mass, radius, and tidal deformability of neutron stars. Constraints from terrestrial experiments have been obtained by studying matter at supra-saturation density in heavy ion collisions and determining the neutron skin thickness. The possibility to detect gravitational waves from merging binary systems by the LIGO and VIRGO collaborations [1,2] and NICER measurements [3,4] on mass radius have major contributions to probe the behavior of the EoS from the low- to the high-density regime. The neutron stars are highly dense asymmetric nuclear systems having a central density about five to six times the nuclear saturation density. In recent years, new measurements of masses from radio pulsars timing [5–7], tidal deformabilities from gravitational wave analyses [1,8] and radii from x-ray pulse profiling [3,4,9,10] have attracted a great deal of attention, as these measurements have started to clarify about the possible existence of the novel state of matter in the dense inner core of the heaviest neutron stars and the EoS of dense matter [11–13]. The nuclear theory studies [14–16] are mainly focusing on understanding the dense matter in a neutron star. The constraints on the EoS at high density are imposed with currently available lower bound on a neutron star's maximum mass and radius [17–19]. The precise measurement of masses of millisecond pulsars such as PSR J1614-2230 [5] and PSR J0348+0432 [6] show that the maximum mass of the neutron star (NS) should be around $2M_{\odot}$. The recent observations with LIGO and Virgo of GW170817 event [1,2] of binary neutron stars merger and the discovery of neutron star with masses around $2M_{\odot}$ [5,6,9,10,20,21] have intensified the interest in these fascinating objects. The analysis of GW170817 has demonstrated the potential of gravitational wave (GW) observations to yield new information related to the limits on neutron-star tidal deformability.

The PSRJ1748-2446ad discovered by Hessels *et al.*, [22] is the fastest spinning pulsar having frequency 716 Hz ($P_s = 1.3959$ ms) and mass $\leqslant 2M_{\odot}$. But, pulsar PSR J0952-0607 was discovered by Bassa *et al.* (2017) [23] with a spin period of $P_s = 1.41$ ms, making it the fastest and heaviest [$M_{\max} = (2.35 \pm 0.17)M_{\odot}$] known galactic neutron star in the disk of the Milky Way. It is a black widow pulsar with a low mass

*raj.phy@gmail.com
†virenthakur2154@gmail.com
‡sinp.bijay@gmail.com
§shashi.dhiman@gmail.com

substellar companion being irradiated and evaporated by the pulsar luminosity. The pulsar J0952-0607 is a particularly attractive candidate for further investigation, as the neutron-star mass is indeed the largest well-measured value [$M_{\rm max} = (2.35 \pm 0.17) M_\odot$] to date. This heaviest observed neutron star for the black widow pulsar should have deep implications on the dense matter EoS. Also with a central value of $2.35 M_\odot$, PSR J0952-0607 provides the most severe constraints on the dense matter EoS [24].

The recent parity-violating electron-scattering experiments on ^{48}Ca (CREX) [25] and ^{208}Pb (PREX-II) [26] are of considerable interest. The PREX I + II combined yield neutron skin thickness for ^{208}Pb as $\Delta r_{np} = 0.283 \pm 0.071$ fm which implies [20] 68% confidence ranges of symmetry energy $J = 38.29 \pm 4.66$ MeV and slope of symmetry energy $L = 109.56 \pm 36.41$ MeV. Both values, and the measured value of neutron skin thickness itself, are considerably larger than from expectations from neutron matter and value of nuclear binding energies, including the previous measurements, although overlapping with them at about the 90% confidence level. This indicates a tension with the current understanding of the EoS. In contrast, the measurement of the neutron skin of ^{48}Ca using the same technique [25] is somewhat smaller than the average of earlier experimental measurements and expectations from nuclear binding energies and neutron matter theory. A Bayesian analysis of the PREX and CREX results is performed in Ref. [27]. They found that the two experimental results are incompatible with each other at 68% confidence level, but compatible at 90% confidence level. Combining the data, they inferred $J = 30.2^{+4.1}_{-3.0}$ MeV and $L = 15.3^{+46.8}_{-41.5}$ MeV at 90% confidence level. They find the combined results predict Δr_{np} for ^{48}Ca close to the CREX result, but predict Δr_{np} for ^{208}Pb considerably smaller than the PREX result. A combined analysis is also performed in Ref. [28] and concludes that a simultaneous accurate description of the skins of ^{48}Ca and ^{208}Pb cannot be achieved with their models that accommodate mass, charge radii, and experimental dipole polarizabilities. The two experiments CREX and PREX-II separately predict incompatible ranges of L, $L = -5 \pm 40$ MeV and $L = 121 \pm 47$ MeV, respectively, but accepting both measurements to be equally valid suggests $J = 32 \pm 2$ MeV and $L = 50 \pm 12$ MeV [29]. The large value of $\Delta r_{np} = 0.283 \pm 0.071$ fm suggests a very stiff EoS and large value of L around saturation density that generally gives rise to a large value of neutron-star radius and the tidal deformability [30]. The upper limit on $\Lambda_{1.4} \leqslant 580$ for GW170817 requires softer EoS and hence softer symmetry energy coefficient [1]. The heaviest neutron star $2.14^{+0.10}_{-0.09} M_\odot$ of PSRJ0740+6620 [7] also strongly limits the symmetry energy under the constraint on the EoS of symmetric nuclear matter (SNM) from flow data in heavy ion collisions [31] which is relatively soft and strongly limits the neutron-star maximum mass. The fastest and heaviest observed galactic neutron star $M_{\rm max} = (2.35 \pm 0.17) M_\odot$ for the black-widow pulsar PSR J0952-0607 [24] may put stringent or severe constraints on the symmetry energy at high densities and on EoS of dense matter. The heaviest observed neutron-star mass for the black widow pulsar demands a stiff EoS and a stiff slope of the symmetry energy coefficient.

The motivation for the present work is to generate new parametrizations for the relativistic mean field (RMF) model that can be used to constrain the EoSs in light of heaviest observed neutron star $M_{\rm max} = (2.35 \pm 0.17) M_\odot$ for the black widow pulsar PSR J0952-0607. The RMF models used in the present work include different combinations of nonlinear, self-couplings, and cross couplings among isoscalar-scalar σ, isoscalar-vector ω_μ, and isovector-vector ρ_μ meson fields for isoscalar and isovector sectors. These parametrizations are to be generated in such a way so that they can accommodate the properties of neutron stars within the astrophysical observations without compromising the finite nuclei and bulk nuclear matter properties. The ω meson self-interaction term ζ plays an important role in determining the soft and stiff behavior of EoS at high densities without affecting the bulk nuclear matter properties at high density. The neutron-star mass decreases with the increase in value of coupling ζ [32–36]. So in order to maintain compatibility with a heaviest neutron-star mass, this self-interaction term is either not incorporated or a very small value is taken in many recent studies which employ the RMF models [37,38]. We also generate a parameter set in accordance with the naturalness behavior as imposed by the effective-field theory [39].

The paper is organized as follows, in Sec. II, a brief outline of the RMF Lagrangian, equations of motion and the EoS for neutron stars is provided. In Sec. III, the procedure for optimization of the model parameters is discussed. Numerical results and detailed discussions concerning features of finite nuclei, bulk nuclear matter, and neutron-star matter are presented in Sec. IV. Finally, we give a summary in Sec. V.

II. THEORETICAL MODEL

The effective Lagrangian density for the RMF model generally describes the interaction of the baryons via the exchange of σ, ω, and ρ mesons up to the quartic order. The Lagrangian density [32,33,38] is given by

$$
\begin{aligned}
\mathcal{L} = & \sum_B \overline{\Psi}_B \Big[i\gamma^\mu \partial_\mu - (M_B - g_{\sigma B}\sigma) - \Big(g_{\omega B}\gamma^\mu \omega_\mu + \frac{1}{2} g_{\rho B}\gamma^\mu \tau_B . \rho_\mu \Big) \Big] \Psi_B + \frac{1}{2}\big(\partial_\mu \sigma \partial^\mu \sigma - m_\sigma^2 \sigma^2\big) \\
& - \frac{\kappa}{3!} g_{\sigma N}^3 \sigma^3 - \frac{\lambda}{4!} g_{\sigma N}^4 \sigma^4 - \frac{1}{4}\omega_{\mu\nu}\omega^{\mu\nu} + \frac{1}{2} m_\omega^2 \omega_\mu \omega^\mu + \frac{1}{4!}\zeta g_{\omega N}^4 (\omega_\mu \omega^\mu)^2 - \frac{1}{4}\rho_{\mu\nu}\rho^{\mu\nu} + \frac{1}{2} m_\rho^2 \rho_\mu \rho^\mu \\
& + \frac{1}{4!}\xi g_{\rho N}^4 (\rho_\mu \rho^\mu)^2 + g_{\sigma N} g_{\omega N}^2 \sigma \omega_\mu \omega^\mu \Big(a_1 + \frac{1}{2} a_2 g_{\sigma N}\sigma \Big) + g_{\sigma N} g_{\rho N}^2 \sigma \rho_\mu \rho^\mu \Big(b_1 + \frac{1}{2} b_2 g_{\sigma N}\sigma \Big) \\
& + \frac{1}{2}\Lambda_v g_{\omega N}^2 g_{\rho N}^2 \omega_\mu \omega^\mu \rho_\mu \rho^\mu - \frac{1}{4} F_{\mu\nu} F^{\mu\nu} - \sum_B e \overline{\Psi}_B \gamma_\mu \frac{1 + \tau_{3B}}{2} A_\mu \Psi_B + \sum_{\ell = e,\mu} \overline{\Psi}_\ell (i\gamma^\mu \partial_\mu - M_\ell) \Psi_\ell . \qquad (1)
\end{aligned}
$$

The equation of motion for baryons, mesons, and photons can be derived from the Lagrangian density defined in Eq. (1). The equation of motion for baryons can be given as

$$\left[\gamma^{\mu}\left(i\partial_{\mu}-g_{\omega B}\omega_{\mu}-\tfrac{1}{2}g_{\rho B}\tau_{B}.\rho_{\mu}-e\tfrac{1+\tau_{3B}}{2}A_{\mu}\right)-(M_{B}+g_{\sigma B}\sigma)\right]\Psi_{B}=\epsilon_{B}\Psi_{B}. \tag{2}$$

The Euler-Lagrange equations for the ground-state expectation values of the mesons fields are

$$\left(-\Delta+m_{\sigma}^{2}\right)\sigma=\sum_{B}g_{\sigma B}\rho_{sB}-\frac{\overline{\kappa}}{2}g_{\sigma N}^{3}\sigma^{2}-\frac{\overline{\lambda}}{6}g_{\sigma N}^{4}\sigma^{3}+a_{1}g_{\sigma N}g_{\omega N}^{2}\omega^{2}+a_{2}g_{\sigma N}^{2}g_{\omega N}^{2}\sigma\omega^{2}+b_{1}g_{\sigma N}g_{\rho B}^{2}\rho^{2}+b_{2}g_{\sigma N}^{2}g_{\rho N}^{2}\sigma\rho^{2}, \tag{3}$$

$$\left(-\Delta+m_{\omega}^{2}\right)\omega=\sum_{B}g_{\omega B}\rho_{B}-\frac{\zeta}{6}g_{\omega N}^{4}\omega^{3}-2a_{1}g_{\sigma N}g_{\omega N}^{2}\sigma\omega-a_{2}g_{\sigma N}^{2}g_{\omega N}^{2}\sigma^{2}\omega-\Lambda_{v}g_{\omega N}^{2}g_{\rho N}^{2}\omega\rho^{2}, \tag{4}$$

$$\left(-\Delta+m_{\rho}^{2}\right)\rho=\sum_{B}g_{\rho B}\tau_{3B}\rho_{B}-\frac{\xi}{6}g_{\rho N}^{4}\rho^{3}-2b_{1}g_{\sigma N}g_{\rho N}^{2}\sigma\rho-b_{2}g_{\sigma N}^{2}g_{\rho N}^{2}\sigma^{2}\rho-\Lambda_{v}g_{\omega N}^{2}g_{\rho N}^{2}\omega^{2}\rho, \tag{5}$$

$$-\Delta A_{0}=e\rho_{p}. \tag{6}$$

where the baryon vector density ρ_B, scalar density ρ_{sB}, and charge density ρ_p are, respectively,

$$\rho_{B}=\langle\overline{\Psi}_{B}\gamma^{0}\Psi_{B}\rangle=\frac{\gamma k_{B}^{3}}{6\pi^{2}}, \tag{7}$$

$$\rho_{sB}=\langle\overline{\Psi}_{B}\Psi_{B}\rangle=\frac{\gamma}{(2\pi)^{3}}\int_{0}^{k_{B}}d^{3}k\frac{M_{B}^{*}}{\sqrt{k^{2}+M_{B}^{*2}}}, \tag{8}$$

$$\rho_{p}=\left\langle\overline{\Psi}_{B}\gamma^{0}\frac{1+\tau_{3B}}{2}\Psi_{B}\right\rangle, \tag{9}$$

with γ the spin-isospin degeneracy. The $M_B^*=M_B-g_{\sigma B}\sigma$ is the effective mass of the baryon species B, k_B is its Fermi momentum, and τ_{3B} denotes the isospin projections of baryon B. The energy density of the uniform matter within the framework of the RMF model is given by

$$\begin{aligned}\mathcal{E}=&\sum_{j=B,\ell}\frac{1}{\pi^{2}}\int_{0}^{k_{j}}k^{2}\sqrt{k^{2}+M_{j}^{*2}}dk+\sum_{B}g_{\omega B}\omega\rho_{B}+\sum_{B}g_{\rho B}\tau_{3B}\rho_{B}\rho+\frac{1}{2}m_{\sigma}^{2}\sigma^{2}+\frac{\overline{\kappa}}{6}g_{\sigma N}^{3}\sigma^{3}+\frac{\overline{\lambda}}{24}g_{\sigma N}^{4}\sigma^{4}-\frac{\zeta}{24}g_{\omega N}^{4}\omega^{4}\\&-\frac{\xi}{24}g_{\rho N}^{4}\rho^{4}-\frac{1}{2}m_{\omega}^{2}\omega^{2}-\frac{1}{2}m_{\rho}^{2}\rho^{2}-a_{1}g_{\sigma N}g_{\omega N}^{2}\sigma\omega^{2}-\frac{1}{2}a_{2}g_{\sigma N}^{2}g_{\omega N}^{2}\sigma^{2}\omega^{2}-b_{1}g_{\sigma N}g_{\rho N}^{2}\sigma\rho^{2}-\frac{1}{2}b_{2}g_{\sigma N}^{2}g_{\rho N}^{2}\sigma^{2}\rho^{2}\\&-\frac{1}{2}\Lambda_{v}g_{\omega N}^{2}g_{\rho N}^{2}\omega^{2}\rho^{2}.\end{aligned} \tag{10}$$

The pressure of the uniform matter is given by

$$\begin{aligned}P=&\sum_{j=B,\ell}\frac{1}{3\pi^{2}}\int_{0}^{k_{j}}\frac{k^{4}dk}{\sqrt{k^{2}+M_{j}^{*2}}}-\frac{1}{2}m_{\sigma}^{2}\sigma^{2}-\frac{\overline{\kappa}}{6}g_{\sigma N}^{3}\sigma^{3}-\frac{\overline{\lambda}}{24}g_{\sigma N}^{4}\sigma^{4}+\frac{\zeta}{24}g_{\omega N}^{4}\omega^{4}\\&+\frac{\xi}{24}g_{\rho N}^{4}\rho^{4}+\frac{1}{2}m_{\omega}^{2}\omega^{2}+\frac{1}{2}m_{\rho}^{2}\rho^{2}+a_{1}g_{\sigma N}g_{\omega N}^{2}\sigma\omega^{2}+\frac{1}{2}a_{2}g_{\sigma N}^{2}g_{\omega N}^{2}\sigma^{2}\omega^{2}\\&+b_{1}g_{\sigma N}g_{\rho N}^{2}\sigma\rho^{2}+\frac{1}{2}b_{2}g_{\sigma N}^{2}g_{\rho N}^{2}\sigma^{2}\rho^{2}+\frac{1}{2}\Lambda_{v}g_{\omega N}^{2}g_{\rho N}^{2}\omega^{2}\rho^{2}.\end{aligned} \tag{11}$$

Here, the sum is taken over nucleons and leptons.

III. PARAMETRIZATION OF THE RELATIVISTIC MEAN-FIELD MODEL

The optimization of the parameters (p) appearing in the Lagrangian (1) has been performed by using the simulated annealing method (SAM) [40,41] by following the χ^2 minimization procedure, which is given as

$$\chi^{2}(\mathbf{p})=\frac{1}{N_{d}-N_{p}}\sum_{i=1}^{N_{d}}\left(\frac{O_{i}^{\mathrm{expt}}-O_{i}^{\mathrm{theor}}}{\sigma_{i}}\right)^{2}, \tag{12}$$

where N_d is the number of experimental data points and N_p is the number of fitted parameters. σ_i denotes adopted errors [42] and O_i^{expt} and O_i^{theor} are the experimental and the corresponding theoretical values, respectively, for a given observable. We search the parameters of the model by fitting the available experimental data of total binding energies and charge rms radii [43–46] for some closed or open-shell nuclei ^{16,24}O, ^{40,48,54}Ca, ^{56,68,78}Ni, ^{88}Sr, ^{90}Zr, ^{100,116,132,138,}Sn, and ^{144}Sm, ^{208}Pb. We have also included the recently measured neutron skin thickness (Δr_{np}) [26] in our fitted data

TABLE I. Newly generated parameter sets HPU1, HPU2, and HPU3 of the RMF Lagrangian given in Eq. (1) along with the theoretical uncertainties. The parameters $\overline{\kappa}$, a_1, and b_1 are in fm^{-1}. The mass for the nucleon and ω and ρ meson is taken as $M_N = 939$ MeV, $m_\omega = 782.5$ MeV, and $m_\rho = 770$ MeV. The values of $\overline{\kappa}$, $\overline{\lambda}$, a_1, a_2, b_1, and b_2 are multiplied by 10^2. Parameters for the DOPS1, NL3, and Big Apple models are also shown for comparison.

Model	HPU1	HPU2	HPU3	DOPS1	NL3	Big Apple
g_σ	9.37959 ± 0.03534	9.91463 ± 0.06587	9.87733 ± 0.06297	10.20651	10.21743	9.67810
g_ω	11.63792 ± 0.06056	12.45333 ± 0.04816	12.45229 ± 0.05479	12.87969	12.86762	12.33541
g_ρ	10.79751 ± 0.80596	10.65758 ± 1.07023	11.34072 ± 2.48071	14.13399	8.94800	14.14256
$\overline{\kappa}$	3.14479 ± 0.17668	2.45494 ± 0.12517	3.10148 ± 0.53829	2.62033	1.95734	2.61776
$\overline{\lambda}$	-2.51218 ± 0.25041	-1.67119 ± 0.18478	-1.57402 ± 0.33738	−1.67616	−1.59137	−2.16586
ζ	–	0.00682 ± 0.23594	0.003301 ± 0.03266	–	–	0.000699
Λ_v	0.05396 ± 0.02277	0.04745 ± 0.02773	0.00248 ± 0.47194	0.00869	–	0.09400
a_1	–	–	0.03559 ± 0.03112	002169	–	–
a_2	–	–	0.01428 ± 0.16366	0.01785	–	–
b_1	–	–	0.47507 ± 1.78695	0.73554	–	–
b_2	–	–	0.92769 ± 0.34847	0.98545	–	–
m_σ	497.976 ± 3.004	501.606 ± 4.346	498.638 ± 5.172	503.620	508.194	492.975

to constrain the linear density dependence of symmetry energy. The maximum mass of the neutron star, $M_{\max} = (2.35 \pm 0.17)M_\odot$ [24], is also included in the fitting protocol. The pairing has been included for the open-shell nuclei by using the BCS formalism with constant pairing gaps that have been taken from the particle separation energies of neighboring nuclei [44,47,48]. The parameter sets are generated in consideration of pulsar PSR J0952-0607 also satisfying finite and bulk nuclear matter properties. The heaviest observed neutron-star mass for the black widow pulsar and PREX-II results demands a stiff EoS and a stiff slope of the symmetry energy coefficient.

We generate three parameter sets for different combinations of nonlinear, self-coupling, and cross coupling among isoscalar-scalar σ, isoscalar-vector ω_μ, and isovector-vector ρ_μ meson fields up to the quartic order as enumerated below:

(i) In the HPU1 parametrization, self-interactions $\overline{\kappa}$, $\overline{\lambda}$ of the σ meson and the cross-interaction term Λ_v of ω^2-ρ^2 mesons, in addition to the exchange interactions of baryons with the σ, ω, and ρ mesons are taken in the Lagrangian. The ω meson self-interaction term ζ is not included in order to maintain compatibility with heaviest observed neutron-star mass $M_{\max} = (2.35 \pm 0.17)M_\odot$ for the black widow pulsar PSR J0952-0607.

(ii) In the HPU2 parametrization, we also incorporate the ω meson self coupling parameter ζ in addition to the coupling terms considered in the HPU1 model.

(iii) In the HPU3 parametrization, we include all possible self-coupling and cross coupling among isoscalar-scalar σ, isoscalar-vector ω_μ, and isovector-vector ρ_μ meson fields up to the quartic order so that this parameter set satisfy the mass constraints of PSR J0952-0607 along with finite nuclear properties and PREX-II results on neutron skin thickness of ^{208}Pb. The inclusion of these possible self- and cross-interaction terms of σ, ω, and ρ mesons are important to accommodate naturalness behavior of parameters as imposed by effective-field theory [39]. In Table I, we display the values of coupling parameters for the HPU1, HPU2, and HPU3 parametrizations generated for the Lagrangian given by Eq. (1) along with the theoretical uncertainties or errors calculated by the method discussed in Refs. [42,49]. The values of parameter sets for DOPS1 [38], NL3 [50], and Big Apple [37] are also shown.

Having obtained the parameters sets, we also calculate the correlation coefficients between two parameters or observables by the covariance analysis, as discussed in Refs. [42,49,51,52]. In Figs. 1–3 we show the plots for the correlation coefficients between the coupling parameters appearing in Lagrangian (1) for the HPU1, HPU2, and HPU3

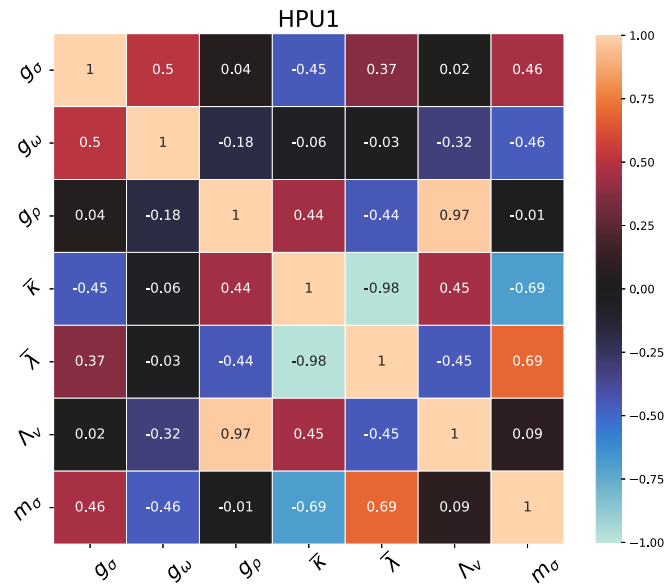

FIG. 1. Correlation coefficients among the model parameters of the Lagrangian given by Eq. (1) for HPU1 parametrization.

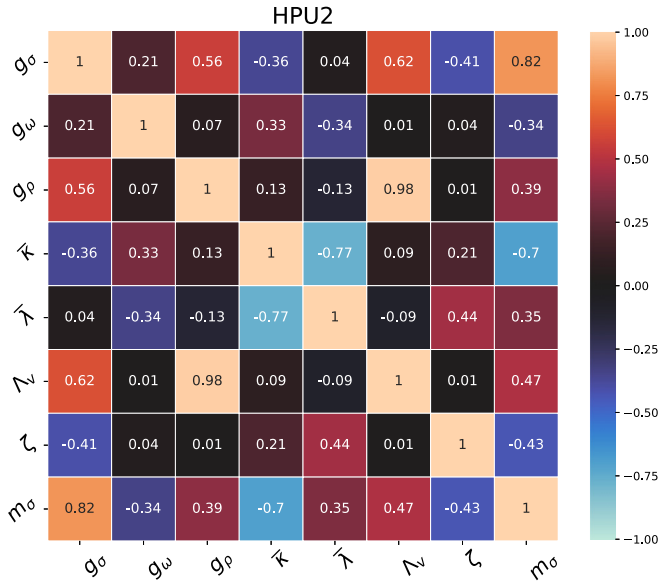

FIG. 2. Same as Fig. 1, but for HPU2 parametrization.

models. It can be observed from Figs. 1 and 2 that a strong correlation exists between the pairs of coupling parameters Λ_v-g_ρ, and $\bar{\kappa}$-$\bar{\lambda}$ for the HPU1 and HPU2 models. In addition, a strong correlation is also observed for pair of coupling parameters g_σ-m_σ for the HPU2 model. It can be observed that, for the HPU3 model, the coupling parameter Λ_v shows a strong dependence on cross-interaction terms. The correlation coefficient between Λ_v and g_ρ becomes weak and Λ_v shows a strong correlation with coupling parameters a_1, a_2, and b_2 and a good correlations with b_1. The isovector coupling parameter g_ρ is found to be strongly correlated with b_1. A

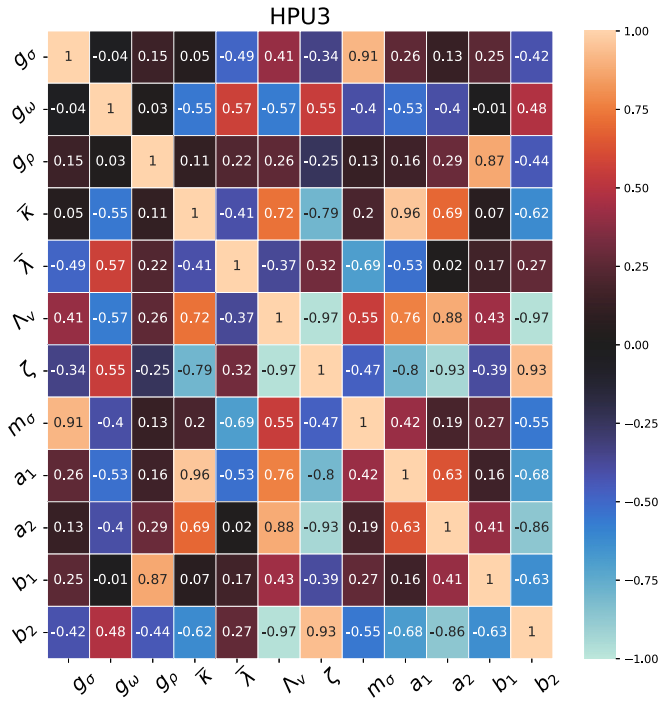

FIG. 3. Same as Fig. 1, but for HPU3 parametrization.

strong correlation between the model parameters indicates a strong interdependence, i.e., if one parameter is fixed at a certain value then the other must attain the precise value as suggested by their correlation. The effective-field theory imposes the condition of naturalness [39] on the parameters or expansion coefficients appearing in the effective Lagrangian density Eq. (1). According to naturalness, the coefficients of various terms in the Lagrangian density functional should be of the same size when expressed in an appropriate dimensionless ratio. The dimensionless ratios are obtained by dividing Eq. (1) by M^4 and expressing each term in powers of $g_\sigma\sigma/M$, $g_\omega\omega/M$, and $2g_\rho\rho/M$. This indicates that the dimensionless ratios $\frac{1}{2C_\sigma^2M^2}$, $\frac{1}{2C_\omega^2M^2}$, $\frac{1}{8C_\rho^2M^2}$, $\frac{\bar{\kappa}}{6M}$, $\frac{\bar{\lambda}}{24}$, $\frac{\zeta}{24}$, $\frac{a_1}{M}$, $\frac{a_2}{2}$, $\frac{b_1}{4M}$, $\frac{b_2}{8}$, and $\frac{\Lambda_v}{8}$ should be roughly the same size, where $C_i^2 = \frac{g_i^2}{m_i^2}$, and i denotes σ, ω, or ρ mesons. In Table II, we display the overall naturalness behavior of HPU's parametrizations, i.e., the value of these coupling parameters when expressed in appropriate dimensionless ratios as discussed above. The corresponding values for the DOPS1, NL3, and Big Apple parameter sets are also shown for sake of comparison. It is obvious from the table that the HPU3 parametrization closely favors the naturalness behavior. This may be attributed to the fact that this parametrization includes possible self- and crossed-interaction terms of σ, ω, and ρ mesons up to the quartic order. The small value of parameter Λ_v (cross interaction term of ω^2 and ρ^2) appearing in Eq. (1) for HPU3 model which might be responsible for better naturalness behavior of the parameters is attributed to the fact that the coupling parameter Λ_v shows strong dependence on the cross-coupling terms a_1, a_2, b_1, and b_2 as suggested by their correlation coefficients (see Fig. 3). It is evident from Table I that the value of coupling parameter Λ_v is relatively larger for HPU1, HPU2, and Big Apple and shows deviation from the naturalness behavior that might be attributed to the fact of not including cross interactions in their respective Lagrangian. It can be seen from Table II that the value of the coupling term Λ_v after expressed in the appropriate dimensionless ratio is 6.745, 5.931, and 11.750 for the HPU1, HPU2, and Big Apple models respectively. Keeping in view the naturalness behavior of the parameters as imposed by the effective-field theory [39] and as observed in the HPU3 model, it can be concluded that cross-interaction terms of mesons have a significant role and their contributions have to be incorporated into the Lagrangian. The naturalness behavior of parameters can be further improved by considering the next higher-order terms containing the gradient of fields [39]. NL3 parametrization favors the naturalness behavior of the parameter but it does not include any cross-interaction terms of ω and ρ mesons, which are very important for constraining the symmetry energy and its density dependence. Also, it is observed from the table that the ω meson coupling term ζ should be either zero or attain a very small value in the calibration procedure of parameters in order to maintain compatibility with the high maximum mass of neutron stars like pulsar PSR J0952-0607.

IV. RESULTS AND DISCUSSION

In this section we use the model parametrizations HPUs to calculate the properties of finite nuclei, bulk nuclear matter, and neutron stars. We also discuss the correlations among nuclear matter observables and model parameters.

TABLE II. The values of parameters are expressed as dimensionless ratios corresponding to naturalness behavior. All values have been multiplied by 10^3.

Parameter	HPU1	HPU2	HPU3	DOPS1	NL3	Big Apple
$\frac{1}{2C_\sigma^2 M^2}$	1.598	1.451	1.445	1.381	1.403	1.469
$\frac{1}{2C_\omega^2 M^2}$	2.564	2.238	2.239	2.093	2.097	2.282
$\frac{1}{8C_\rho^2 M^2}$	0.721	0.7406	0.654	0.421	1.031	0.412
$\frac{\bar{\kappa}}{6M}$	1.101	0.860	1.086	0.918	0.668	0.917
$\frac{\bar{\lambda}}{24}$	−1.047	−0.696	−0.656	−0.698	−0.663	−0.902
$\frac{\zeta}{24}$	–	0.284	0.138	–	–	0.029
$\frac{a_1}{M}$	–	–	0.356	0.217	–	–
$\frac{a_2}{2}$	–	–	0.101	0.089	–	–
$\frac{b_1}{4M}$	–	–	1.187	1.839	–	–
$\frac{b_2}{8}$	–	–	1.159	1.232	–	–
$\frac{\Lambda_v}{8}$	6.745	5.931	0.310	1.086	–	11.750

A. Properties of finite nuclei and nuclear matter

The newly generated parametrizations HPU1, HPU2, and HPU3 give a good fit to the properties of finite nuclei. The binding energies obtained using HPUs parametrizations are in harmony with the available experimental data [43,44]. The value of rms errors in the total binding energies calculated for the HPU1, HPU2, and HPU3 parametrizations are 3.06, 1.81, and 2.35 MeV, respectively. The root mean square (rms) errors in charge radii for all nuclei taken in our fit are 0.050, 0.016, and 0.017 fm for HPU parameter sets, respectively. The neutron skin thickness for ^{208}Pb comes out to be 0.216, 0.218, and 0.217 fm for HPU1, HPU2, and HPU3 parametrizations, respectively, and is in close proximity with the limits imposed by the PREX-II results [26]. The value of neutron skin thickness of $\Delta r_{np}(^{48}\mathrm{Ca})$ obtained for these parametrizations is consistent with the results reported in Ref. [28].

In Table III, we present the results for the SNM properties such as binding energy per nucleon (E/A), incompressibility (K), the effective nucleon mass (M^*) at the saturation density (ρ_0), the symmetry energy coefficient (J), the slope of symmetry energy (L), and curvature parameter K_{sym}. These SNM properties play an important role for constructing the EoS for nuclear matter. The results are also compared with the DOPS1 [38], NL3 [50], and Big Apple [37] parameter sets. E/A lies in the range of 16.062–16.298 MeV for HPU parametrization. The values of J and L obtained by HPU parametrizations are consistent with the values $J = 38.1 \pm 4.7$ MeV and $L = 106 \pm 37$ MeV, as inferred by Reed *et al.* [30], and is also consistent with the constraints from the observational analysis $J = 31.61 \pm 2.66$ MeV and $L = 58.9 \pm 16$ MeV [53]. The slope of the symmetry energy obtained for the HPU1 parameter set also satisfies the recently reported limit $L = 54 \pm 8$ MeV [54] and $L = 15.3^{+46.8}_{-41.5}$ MeV [27]. The value of K is in the range 225.56–229.88 MeV, which is in agreement with the value $K = 240 \pm 20$ MeV determined from isoscalar giant monopole resonance (ISGMR) for ^{90}Zr and ^{208}Pb nuclei [55,56]. The value of the

TABLE III. The bulk nuclear matter properties (NMPs) at saturation density for HPU parametrization compared with that of other parameter sets. ρ_0, E/A, K, M^*/M, J, L, and K_{sym} denote the saturation density, binding energy per nucleon, nuclear matter incompressibility coefficient, the ratio of effective nucleon mass to the nucleon mass, the symmetry energy, the slope of the symmetry energy, and the curvature of symmetry energy, respectively. The value of ρ_0 is in fm^{-3} and all of the rest of the quantities are in MeV. The values of neutron skin thickness Δr_{np} for ^{208}Pb and ^{48}Ca nuclei in units of fm are also listed.

NMPs	HPU1	HPU2	HPU3	DOPS1	NL3	Big Apple
ρ_0	0.157	0.150	0.151	0.150	0.148	0.155
E/A	−16.298	−16.119	−16.062	−16.073	−16.248	−16.339
K	229.88	225.84	225.56	231.20	271.56	227.09
M^*/M	0.639	0.621	0.635	0.604	0.595	0.608
J	34.34	33.21	33.22	31.89	37.40	31.41
L	61.21	63.87	75.03	65.59	118.56	40.34
K_{sym}	−96.85	−70.78	−31.42	18.01	100.90	89.58
Δr_{np} (^{208}Pb)	0.216	0.218	0.217	0.185	0.279	0.150
Δr_{np} (^{48}Ca)	0.202	0.201	0.203	0.182	0.226	0.168

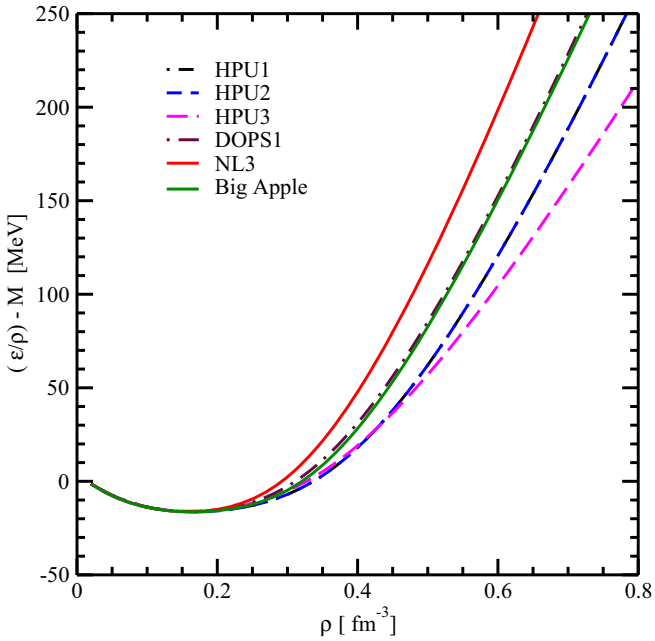

FIG. 4. Binding energy per nucleon in the symmetric nuclear matter as a function of baryon density for various parametrizations considered in the present work.

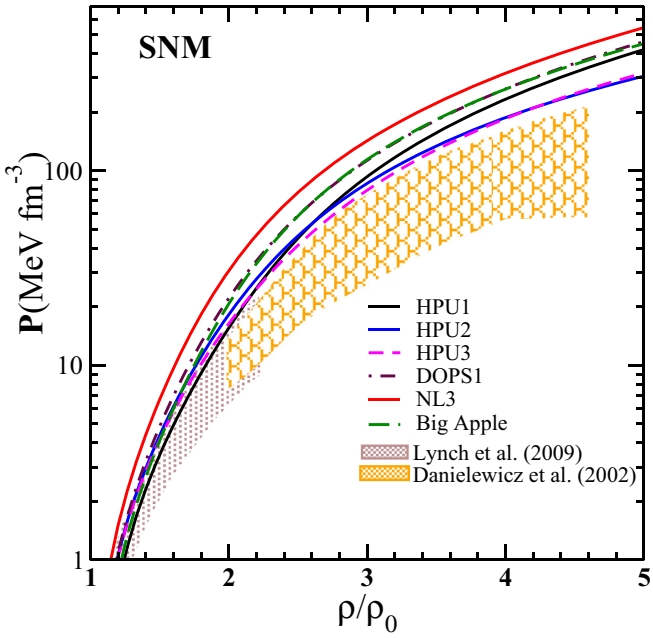

FIG. 5. Pressure as a function of baryon density for symmetric nuclear matter calculated with HPU parametrizations along with DOPS1, NL3, and Big Apple models. The shaded regions represent the experimental data taken from the Refs. [31,64].

curvature of the symmetry energy $K_{\rm sym}$ for HPUs parameter sets also satisfies the empirical limit discussed in Ref. [57]. The value of $K_{\rm sym}$ is determined only poorly [58–60] and the experimental data on finite nuclei is not enough to constrain $K_{\rm sym}$. Only the accurate knowledge of symmetry energy at higher densities ($\rho > 2\rho_0$) may constrain the $K_{\rm sym}$ in tighter bounds. This may be attributed to the large experimental error on the neutron skin thickness for ^{208}Pb (0.283 ± 0.071 fm) which lead us to choose the large adopted error during the optimization procedure. The values of neutron-skin thickness (Δr_{np}) for ^{208}Pb and ^{48}Ca nuclei are also displayed in Table III. It can be observed from the Tables I and III that the slope of the symmetry energy (L) has a strong dependence on the cross-interaction term Λ_v of ω^2–ρ^2 mesons. The value of L decreases with increasing Λ_v. As the value of coupling Λ_v increases from 0.00248 (HPU3) to 0.09400 (Big Apple), the corresponding value of L decreases from 75.03 MeV to 40.34 MeV. For NL3 parameter set, the value of L is large (118.56 MeV), may be due to not including the cross interaction term Λ_v. The values of the symmetry energy coefficient J at $2\rho_0$ for HPU1, HPU2, HPU3 are found to be 53.15, 53.40, and 57.59 MeV, respectively, and are consistent with the constraints $J(2\rho_0) = 51 \pm 13$ MeV inferred from nine new analyses of neutron-star observables since GW170817 [61] and $J(2\rho_0) = 62.8 \pm 15.9$ MeV [62]. The value of J at $2\rho_0$ for HPU1 and HPU2 models are very close to the constraint $J(2\rho_0) = 40.2 \pm 12.8$ MeV based on microscopic calculations with various energy density functionals [63]. The value J at $2\rho_0$ for DOPS1, NL3, and Big Apple models comes out to be 55.23, 78.31, and 49.96 MeV, respectively. Like the slope of symmetry energy (L), J at $2\rho_0$ also shows a similar trend with cross interaction coupling Λ_v. In Fig. 4, we illustrate the binding energy per nucleon $E_B = (\mathcal{E}/\rho) - M$, as a function of baryon density for symmetric nuclear matter for various parametrizations. E_B near saturation density is almost similar for all models considered here but shows significant difference at higher densities. As seen from the figure, the HPU1, DOPS1, and NL3 parametrizations show stiff behavior (large E_B) whereas HPU2 and HPU3 parameters show soft behavior (small E_B) at higher density regions. It may be due to the absence and presence of ω meson coupling parameter in the Lagrangian of the respective parametrization. In Figs. 5 and 6, we plot the EoS, i.e., pressure as a function of baryon density scaled to the saturation density for SNM and PNM using the HPUs parametrizations. Similar results are also shown for the NL3, DOPS1, and Big Apple models. The shaded regions represent the experimental data taken from Refs. [31,64]. The EoS calculated by using the HPU parametrizations are relatively stiffer, which is a requirement to constrain the recent astrophysical observations [24]. It is evident from Fig. 5 that, in the low-density regime (up to $2\rho_0$), the EoSs for SNM obtained for HPUs parametrizations are close to the upper limit of the allowed region with the EoS extracted from the analysis of the particle flow in heavy ion collisions [31] and lie in the upper portion of the allowed region of the EoS extracted from Ref. [64]. After $2\rho_0$, the SNM pressure for all HPU's parametrizations considered in the present work start deviating from the collective flow constraining band. This might be attributed to the fact that these parametrizations are obtained keeping in view the heaviest observed neutron star $M_{\rm max} = 2.35 \pm 0.17 M_\odot$ for the black widow pulsar PSR J0952-0607 and demands a stiff EoSs, i.e., larger value of pressure at higher densities. Also, it can be

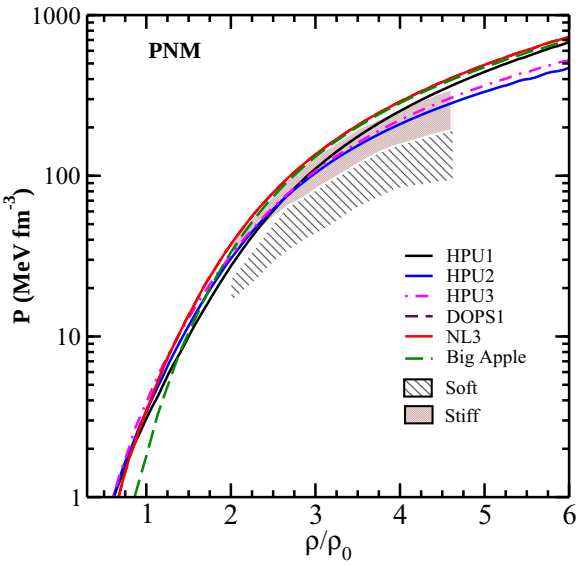

FIG. 6. Variation of pressure as a function of baryon density for pure neutron matter computed with HPUs parametrizations along with DOPS1, NL3, and Big Apple models. The shaded region represents the experimental data taken from the Ref. [31].

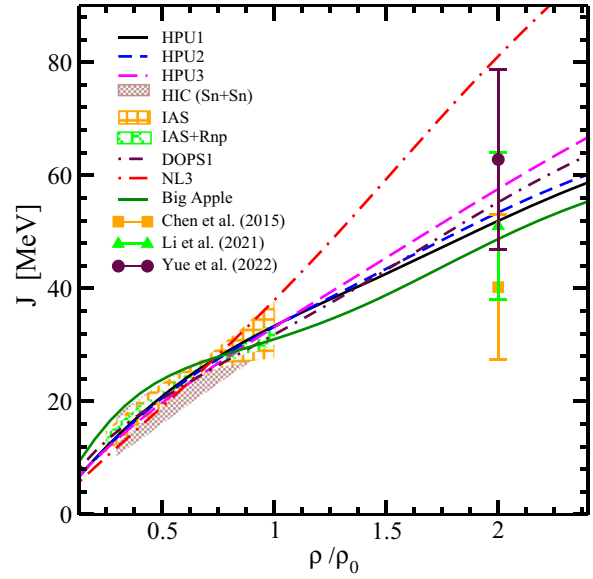

FIG. 7. Symmetry energy as a function of baryon density for various models considered in the present work. The shaded regions represent the constraints on the density dependence of the symmetry energy from heavy ion collisions and isobaric analysis states (IASs) taken from Refs. [65,66]. The constraints on the magnitude of the symmetry energy coefficient at $J(2\rho_0) : J(2\rho_0) = 62.8 \pm 15.9$ MeV [62], $J(2\rho_0) = 51 \pm 13$ MeV from nine new analyses of neutron-star observables since GW170817 [61] and $J(2\rho_0) = 40.2 \pm 12.8$ MeV based on microscopic calculations with various energy density functionals [63] are also shown.

seen from Fig. 6 that the EoSs obtained for PNM using the HPU parameter sets lie in the allowed stiff region. The HPU parametrizations demand stiff EoSs, whereas the prediction of neutron-star maximum mass around $2M_\odot$ and constraints on EoSs of SNM and PNM as extracted from the analysis of particle flow in heavy ion collisions [31] require relatively softer EoSs, as demanded by GW170817 event [31]. It is evident from the figures that the EoSs for SNM and PNM calculated with the NL3, DOPS1, and Big Apple parametrizations are very stiff and follow the similar behavior as followed by the HPU models. In Fig. 7, we plot the symmetry energy as a function of baryon density for various HPU parametrizations. The results for other models are also shown for comparison. The shaded regions represent the constraints on density dependence of symmetry energy from heavy ion collisions and isobaric analog states (IASs) taken from Refs. [65,66]. The constraints on magnitude of symmetry energy coefficient at $J(2\rho_0) : J(2\rho_0) = 62.8 \pm 15.9$ MeV [62], $J(2\rho_0) = 51 \pm 13$ MeV from nine new analyses of neutron-star observables since GW170817 [61], and $J(2\rho_0) = 40.2 \pm 12.8$ MeV based on microscopic calculations with various energy density functionals [63] are also shown. It can be observed that the symmetry energy increases with baryon density for various models considered in the present work and also lie in the allowed regions and satisfy various constraints as discussed above. Among HPU parametrizations, the value of J is found to be stiffest for the HPU3 model and softest for the HPU1 model in the higher-density regime. This might be due to the smaller value of coupling Λ_v in case of HPU3 as compared with its value for HPU1, as this coupling term plays an important role for constraining the symmetry energy and its density dependence.

B. Neutron-star properties

In Fig. 8, we display the EoS, i.e., pressure as a function of energy density for the β-equilibrated nucleonic matter for HPU parametrizations. Similar results are also shown for the DOPS1, NL3, and Big Apple parameter sets. The shaded region (magenta) represents the observational constraints at $r_{ph} = R$ with the 2σ uncertainty [67]. Here r_{ph} and R are the photospheric and neutron-star radius, respectively, and the regions (brown and gray) represent the EoS of cold dense matter with 95% confidence limit reported in Ref. [68]. It can be observed that the EoSs computed with the HPU2 and HPU3 parametrizations are relatively softer and lie in the allowed regions that represent the observational constraints on EoSs reported in Refs. [67,68]. The EoSs obtained by HPU1, DOPS1, NL3, and Big Apple models are showing stiff behavior and are ruled out by the shaded regions shown in Fig. 8. The stiff behavior of EoSs for these parametrizations may be attributed to the fact the ω meson self-coupling term ζ is either not included (HPU1, DOPS1, and NL3) or has a very small value (Big Apple). This is in accordance with the understanding that the coupling term ζ is responsible for softening the EoS at high densities [33,35,36]. Among the HPU models, the EoS for the HPU2 parametrization is found to be relatively softer at higher densities (Fig. 8), which might be attributed to the value of the coupling ζ which is somewhat larger as compared with other parametrizations. The mass and radius of a neutron star are obtained by solving the

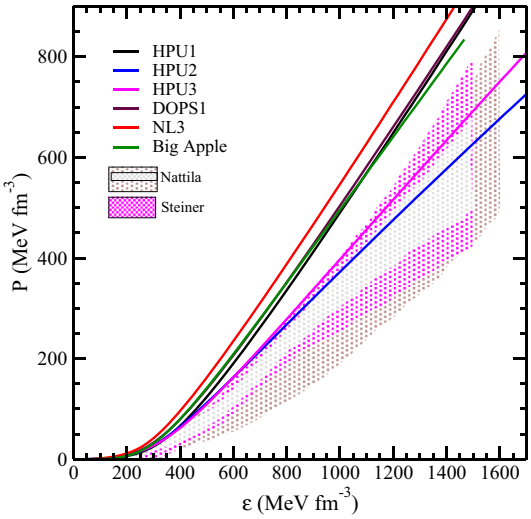

FIG. 8. EoSs, i.e., variation of pressure as a function of energy density for different models considered in the present work. The shaded region (magenta) represents the observational constraints taken from Ref. [67] and the regions (brown and gray) represent the EoS of cold dense matter with a 95% confidence limit [68].

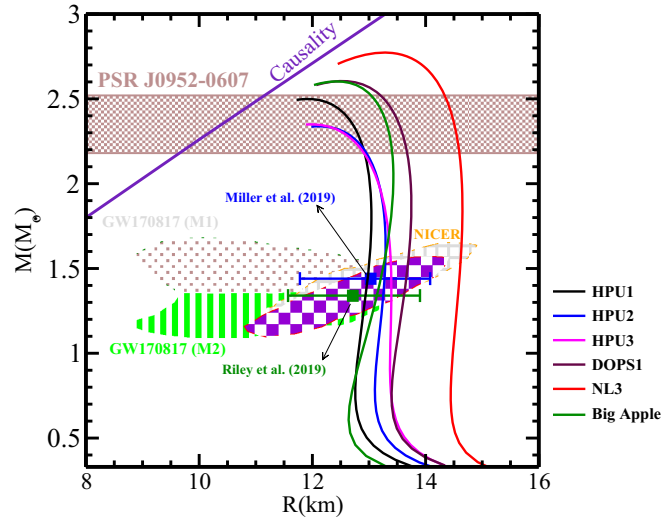

FIG. 9. Neutron-star mass-radius relation for various HPU parametrizations. Horizontal bands correspond to mass $M = (2.35 \pm 0.17)M_\odot$ of PSR J0952-0607 [24]. The mass-radius estimates of the two companion neutron stars in the merger event GW170817 [1] are shown by shaded regions labeled with GW170817 $M1$ ($M2$) along with the constraints from NICER observations [3,4]. The results are shown for the DOPS1, NL3, and Big Apple parameter sets.

Tolman-Oppenheimer-Volkoff (TOV) equations [69,70] given as

$$\frac{dP(r)}{dr} = -\frac{\{\epsilon(r) + P(r)\}\{4\pi r^3 P(r) + m(r)\}}{r^2[1 - 2m(r)/r]} \tag{13}$$

$$\frac{dm}{dr} = 4\pi r^2 \epsilon(r), \tag{14}$$

$$m(r) = 4\pi \int_0^r dr r^2 \epsilon(r), \tag{15}$$

where $P(r)$ is the pressure at radial distance r and $m(r)$ is the mass of the neutron star enclosed in a sphere of radius r. The radius of a canonical neutron star is more sensitive to the EoS of the crust region than those of maximum-mass configurations. For lower densities, we employed Baym-Pethick-Sutherland (BPS) [71] matching on the model EoS at $\rho = 0.5\rho_0$ and going down to 6.0×10^{-12} fm^{-3}. At densities larger than $0.5\rho_0$ we use the model EoS obtained by nucleonic and leptonic contributions. In Fig. 9, we present the results for the gravitational mass of static neutron stars and its radius for the HPU1, HPU2, and HPU3 parametrizations. Similar results calculated for other parameter sets are also displayed. The horizontal bands correspond to mass $M = 2.35 \pm 0.17M_\odot$ of PSR J0952-0607 [24]. The mass-radius estimates of the two companion neutron stars in the merger event GW170817 [1] are shown by the shaded regions labeled GW170817 $M1$ ($M2$). The shaded regions depicting the NICER observations [3,4] are also shown. It is observed that the maximum gravitational mass of the static neutron star for the HPU1, HPU2, and HPU3 parameter sets lie in the range $2.34M_\odot$–$2.50M_\odot$, which is in good agreement with the mass constraints reported for heaviest neutron star, $M_{\rm max} = 2.35 \pm 0.17M_\odot$, for the black widow pulsar PSR J0952-0607 [24]. The HPU parametrizations also satisfy the mass-radius estimates of the two companion neutron stars as inferred in the merger event GW170817 [1], as shown by the shaded regions labeled GW170817 $M1$ ($M2$). The neutron star mass-radius computed by using the HPU parametrizations are in good agreement with the NICER measurements [3,4]. The radius $R_{1.4}$ corresponding to a $1.4M_\odot$ neutron star lie in the range 12.96–13.39 km for the HPU parametrizations and is entirely consistent with the inferences on the radius constraints from NICER [3,4,72]. The radius of $2.08M_\odot$ neutron star lies in the range 12.98 −13.09 km for the HPU parameter sets and is in good agreement with the value predicted: $R_{2.08} = 13.7^{+2.6}_{-1.5}$ km from Miller *et al.* [3] and $R_{2.08} = 12.39^{+1.30}_{-0.98}$ km from Riley *et al.* [4].

The tidal deformability Λ rendered by the companion stars on each other in a binary system can provide remarkable pieces of information on the EoS of neutron stars [73,74]. The tidal influences of its companion in BNS system will deform neutron stars in the binary system, and the resulting change in the gravitational potential modifies the BNS orbital motion and its corresponding gravitational wave (GW) signal. This effect on GW phasing can be parametrized by the dimensionless tidal deformability parameter, $\Lambda_i = \lambda_i/M_i^5$, $i = 1, 2$. For each neutron star, its quadrupole moment $\mathcal{Q}_{j,k}$ must be related to the tidal field $\mathcal{E}_{j,k}$ caused by its companion as $\mathcal{Q}_{j,k} = -\lambda\mathcal{E}_{j,k}$, where j and k are spatial tensor indices. The dimensionless tidal deformability parameter Λ of a static, spherically symmetric compact star depends on the neutron-star compactness parameter C and a dimensionless quadrupole Love number k_2 as $\Lambda = \frac{2}{3}k_2C^{-5}$. The Λ critically parametrizes the deformation of neutron stars under the given tidal field, therefore it should depend on the EoS of nuclear dense matter. To measure the Love number k_2 along with the evaluation of the TOV equations we have to compute $y_2 = y(R)$ with initial boundary condition $y(0) = 2$ from the first-order differential

equation [73–76] simultaneously,

$$y' = \frac{1}{r}[-r^2Q - ye^{\lambda}\{1 + 4\pi Gr^2(P - \mathcal{E})\} - y^2], \quad (16)$$

$$Q \equiv 4\pi Ge^{\lambda}\left(5\mathcal{E} + 9P + \frac{\mathcal{E} + P}{c_s^2}\right) - 6\frac{e^{\lambda}}{r^2} - \nu'^2, \quad (17)$$

$$e^{\lambda} \equiv \left(1 - \frac{2Gm}{r}\right)^{-1}, \quad (18)$$

$$\nu' \equiv 2Ge^{\lambda}\left(\frac{m + 4\pi Pr^3}{r^2}\right). \quad (19)$$

First, we get the solutions of Eq. (16) with boundary condition, $y_2 = y(R)$, then the electric tidal Love number k_2 is calculated from the expression as

$$k_2 = \frac{8}{5}C^5(1-2C)^2[2C(y_2-1) - y_2 + 2]\Big\{2C[4(y_2+1)C^4 + (6y_2-4)C^3 + (26-22y_2)C^2 + 3(5y_2-8)C - 3y_2 + 6] - 3(1-2C)^2[2C(y_2-1) - y_2 + 2]\ln\left(\frac{1}{1-2C}\right)\Big\}^{-1}. \quad (20)$$

The value of $\Lambda_{1.4}$ obtained for canonical mass with HPUs parameter sets lies in the range 610.7–719.0, which satisfies the value obtained from the GW170817 event [8,30,77] for the EoS of dense nuclear matter.

Furthermore, note that the our analysis of tidal deformability ($\Lambda_{1.4}$) lies within the constraints ($\Lambda_{1.4} \leqslant 800$) for GW170817 event [8], $\Lambda_{1.4} = 575^{+262}_{-232}$ [78] using the Miller *et al.* [3] posteriors and $\Lambda_{1.4} = 457^{+219}_{-256}$ [79] using those of Riley *et al.* [4]. The value of $\Lambda_{1.4}$ obtained for the HPU1 model is very close to the upper limit with a revised limit $\Lambda_{1.4} \leqslant 580$ within 1σ uncertainty [1]. The precise measurement of tidal deformability can constrain the neutron-star radius in narrow bounds. Indeed it is believed that no terrestrial experiment can reliably constrain the EoS of a neutron star [30]. In Table IV, we summarize the results for the various properties of neutron stars obtained with the HPU1, HPU2, and HPU3 parametrizations. The results obtained with other parameter sets are also shown for comparison.

TABLE IV. The properties of nonrotating neutron stars obtained for the various parametrizations considered in the present work. $M_{\max}$ and $R_{\max}$ denote the maximum gravitational mass and corresponding radius, respectively. The values for $R_{1.4}$ and $\Lambda_{1.4}$ denote the radius and dimensionless tidal deformability at $1.4M_{\odot}$ and $R_{2.08}$ denotes the radius at $2.08M_{\odot}$.

EoS	M ($M_{\odot}$)	$R_{\max}$ (km)	$R_{1.4}$ (km)	$R_{2.08}$ (km)	$\Lambda_{1.4}$
HPU1	2.50	11.93	12.96	12.98	610.7
HPU2	2.34	12.06	13.26	13.09	699.8
HPU3	2.35	11.97	13.39	13.07	719.0
DOPS1	2.61	12.33	13.64	13.71	770.0
NL3	2.77	12.93	14.59	14.62	1241.6
Big Apple	2.60	12.25	13.18	13.42	715.51

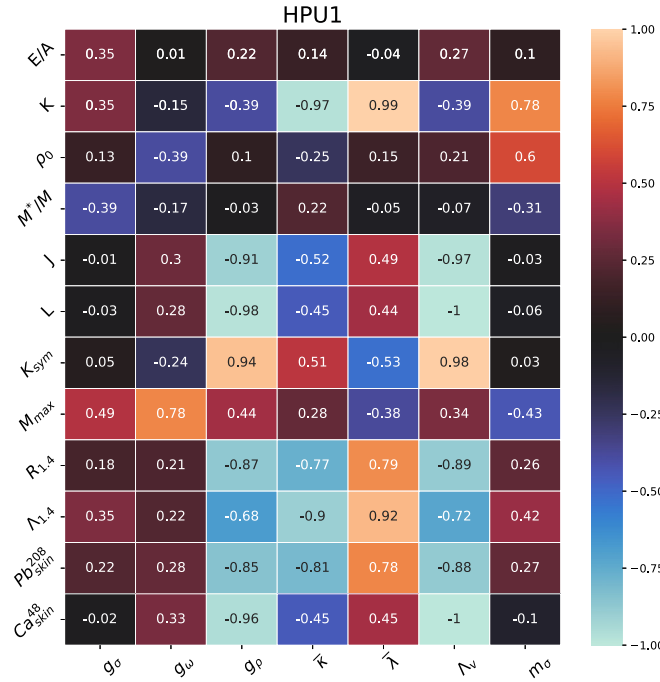

FIG. 10. Correlation coefficients among neutron-star properties as well as the bulk properties of nuclear matter at the saturation density and model parameters for HPU1 parametrization.

C. Correlations among nuclear-matter observables and model parameters

In this section, we discuss the correlations between the bulk nuclear matter and neutron-star observables and model parameters. In Figs. 10–12, we display the correlations of bulk nuclear matter properties at saturation density and neutron-star observables with the model parameters for the HPU parametrizations.

For the HPU1 model, the isoscalar nuclear matter properties K show strong correlations with isoscalar parameters $\overline{\kappa}$ and $\overline{\lambda}$. It can also be observed from Fig. 10 that the J, L, and $K_{\rm sym}$ can be very well constrained by the coupling parameter g_{ρ} and Λ_v, as depicted by their correlations. The neutron-star observables $R_{1.4}$ and $\Lambda_{1.4}$ also show strong dependence on couplings Λ_v and g_{ρ}. The neutron skin thickness of ^{208}Pb and ^{48}Ca also shows strong correlation with Λ_v and g_{ρ} for the HPU1 and HPU2 models. For the HPU2 model, the isoscalar nuclear matter property E/A shows good correlation with isoscalar parameters g_{σ}, and K is strongly correlated with $\overline{\kappa}$. It is evident from Fig. 11 that the isovector properties such as J, L, $K_{\rm sym}$ and neutron-star observables $R_{1.4}$ and $\Lambda_{1.4}$ have a strong dependence on g_{ρ} and Λ_v, as suggested by their correlations. A strong negative correlation is observed for neutron-star maximum mass $M_{\max}$ with coupling ζ, which is well consistent with the findings reported in Refs. [33,35,36], which indicates that the value of ζ is either zero or very small for supporting the hypermassive neutron star. For the HPU3 model, the isovector properties such as J, L, and $K_{\rm sym}$ show a

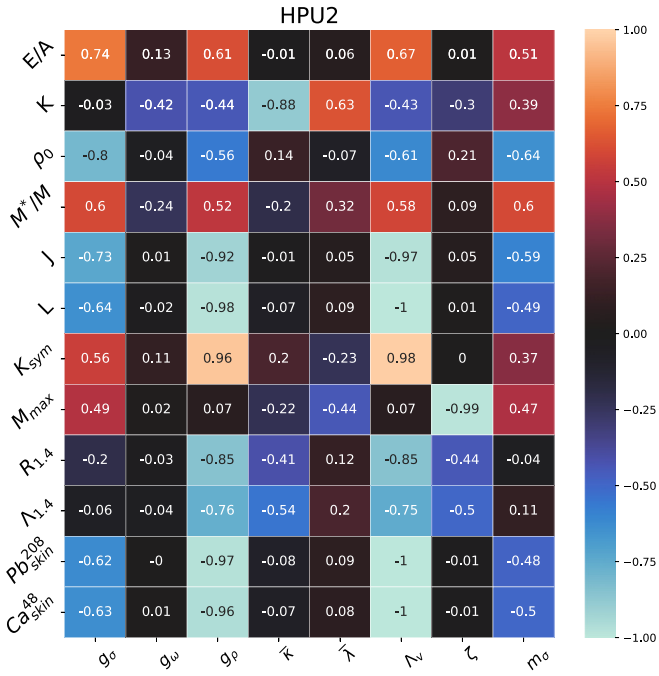

FIG. 11. Same as Fig. 10, but for HPU2 parametrization.

weak correlation with coupling g_ρ. J is found to be strongly correlated with a_1 and a_2 and shows moderate correlation with b_2. $K_{\rm sym}$ also shows good dependence on cross-interaction terms a_1, a_2, and b_2. The neutron-star observables such as $R_{1.4}$ and $\Lambda_{1.4}$ show a good correlations with couplings a_1, a_2, and b_2 and weak correlation with g_ρ. It may be noticed from Fig. 12 that observables such as J, L, $K_{\rm sym}$, $R_{1.4}$, and $\Lambda_{1.4}$ show moderate-to-good correlations with cross-coupling

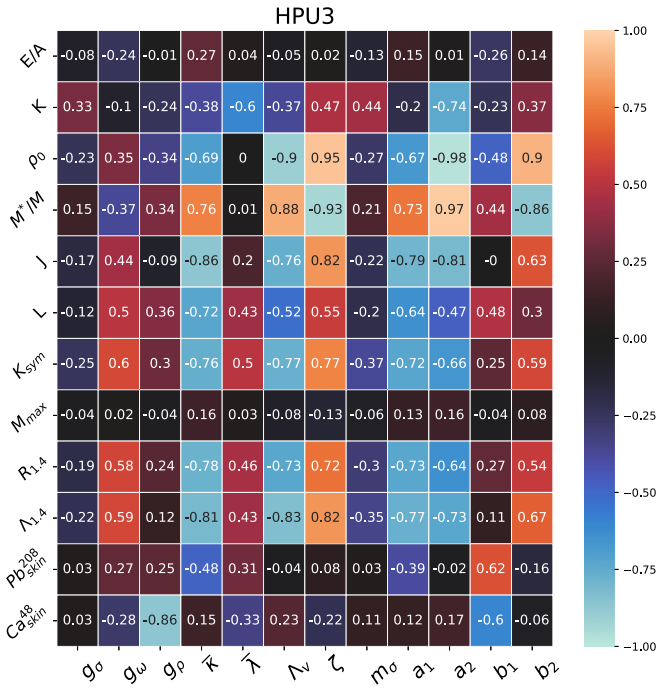

FIG. 12. Same as Fig. 10, but for HPU3 parametrization.

terms incorporated in the HPU3 model. The neutron skin thickness of ^{208}Pb and ^{48}Ca also shows a good dependence on coupling b_1.

V. SUMMARY

Three new parametrizations, namely, HPU1, HPU2, and HPU3 for the RMF model have been generated in the light of the heaviest observed neutron star for the black widow pulsar PSR J092-0607, astrophysical constraints and naturalness behavior of the coupling parameters as demanded by effective-field theory in addition to those usually employed, such as binding energy, charge radii for finite nuclei, and empirical data on the nuclear matter at the saturation density. We have taken different combinations of nonlinear, self-, and cross-interaction terms between σ, ω, and ρ mesons up to the quartic order in the Lagrangian RMF model. The newly generated HPU parametrizations of the RMF model can accommodate the properties of NSs within the astrophysical observations without compromising the finite nuclei and bulk nuclear matter properties. In the HPU1 parametrization, self-interaction terms $\overline{\kappa}$, $\overline{\lambda}$ of σ meson and the cross-interaction term Λ_v of ω-ρ mesons, in addition to the exchange interactions of baryons with σ, ω, and ρ mesons are taken in the Lagrangian. The ω meson self-interaction term ζ is not included in order to maintain compatibility with heaviest observed neutron-star mass $M_{\rm max} = (2.35 \pm 0.17)M_\odot$ for the black widow pulsar PSR J0952-0607. For the HPU2 parametrization, we also incorporate the ω meson self-coupling parameter ζ in addition to the coupling terms considered in the HPU1 model. In the HPU3 parametrization, we include all possible self- and cross-couplings among isoscalar-scalar σ, isoscalar-vector ω_μ, and isovector-vector ρ_μ meson fields up to the quartic order so that the parameter set generated satisfies the mass constraints of PSR J0952-0607. The inclusion of these possible self- and cross-interaction terms are important to accommodate the naturalness behavior of parameters, as imposed by effective-field theory [33,39]. All HPU parametrizations are obtained such that it reproduces the ground-state properties of the finite nuclei, the bulk properties of nuclear matter, and the constraints of mass from the heaviest observed neutron star from the black widow pulsar [24]. We notice that the nonlinear ω meson self-coupling ζ is either very small (HPU2, HPU3) or zero for HPU1 interactions to support a hypermassive neutron star. The root mean square errors in the total binding energies for finite nuclei included in our fit for HPU parametrizations are 3.06, 1.81, and 2.35 MeV, respectively. The root mean square errors in the charge rms radii for the nuclei included in our fit are 0.050, 0.016, and 0.017 fm, respectively. The bulk nuclear matter properties obtained are well consistent with the current empirical data [30,53,56]. The maximum gravitational mass of the neutron star for the HPU parameter sets lie in the range $2.34M_\odot$–$2.50M_\odot$ and is in accordance with the heaviest observed neutron star from the black widow pulsar PSR J0952-0607. The radius $R_{1.4}$ of the neutron star lies in the range 12.96–13.39 km and is in good agreement with the results reported in Refs. [3,4,9,10,72]. The value of $\Lambda_{1.4}$ obtained for the HPU parametrizations

lies in the range 610.7–719.0 and also satisfies the constraints for the GW170817 event [8] and reported in Refs. [30,77–79].

The parametrizations generated in light of PSR J0952-0607 demands stiff EoSs, leading to the relatively larger value of $\Lambda_{1.4}$. To satisfy the revised limit of tidal deformability, $\Lambda_{1.4} \leqslant 580$ [1], the softening of the EoS at intermediate densities together with the subsequent stiffening in high-density regions is required to support massive neutron stars that may be indicative of a phase transition in the stellar core [80].

ACKNOWLEDGMENTS

Author(s) are thankful to Himachal Pradesh University for providing the computational facility. B.K.A. acknowledges partial support from the SERB, Department of Science and Technology, Govt. of India with Grants No. SIR/2022/000566 and No. CRG/2021/000101 respectively. S.K. is highly thankful to CSIR-UGC (Govt. of India) for providing financial assistance (NTA/ 211610029883 dated 19/04/2022) under the Junior/Senior Research Fellowship scheme.

[1] B. P. Abbott, R. Abbott, T. D. Abbott, F. Acernese, K. Ackley, C. Adams, T. Adams, P. Addesso, R. X. Adhikari, V. B. Adya *et al.*, GW170817: Measurements of Neutron Star Radii and Equation of State, Phys. Rev. Lett. **121**, 161101 (2018).

[2] B. P. Abbott, R. Abbott, T. D. Abbott, F. Acernese, K. Ackley, C. Adams, T. Adams, P. Addesso, R. X. Adhikari, V. B. Adya *et al.*, Properties of the Binary Neutron Star Merger GW170817, Phys. Rev. X **9**, 011001 (2019).

[3] M. C. Miller, F. K. Lamb, A. J. Dittmann, S. Bogdanov, Z. Arzoumanian, K. C. Gendreau, S. Guillot, W. C. G. Ho, J. M. Lattimer, M. Loewenstein, S. M. Morsink, P. S. Ray, M. T. Wolff, C. L. Baker, T. Cazeau, S. Manthripragada, C. B. Markwardt, T. Okajima, S. Pollard, I. Cognard, H. T. Cromartie, E. Fonseca, L. Guillemot, M. Kerr, A. Parthasarathy, T. T. Pennucci, S. Ransom, and I. Stairs, The radius of PSR J0740 + 6620 from NICER and XMM-newton data, Astrophys. J. Lett. **918**, L28 (2021).

[4] T. E. Riley, A. L. Watts, P. S. Ray, S. Bogdanov, S. Guillot, S. M. Morsink, A. V. Bilous, Z. Arzoumanian, D. Choudhury, J. S. Deneva *et al.*, A nicer view of the massive pulsar PSR J0740 + 6620 informed by radio timing and XMM-Newton spectroscopy, Astrophys. J. Lett. **918**, L27 (2021).

[5] P. B. Demorest, T. Pennucci, S. M. Ransom, M. S. E. Roberts, and J. W. T. Hessels, A two-solar-mass neutron star measured using Shapiro delay, Nature (London) **467**, 1081 (2010).

[6] J. Antoniadis, P. C. C. Freire, N. Wex, T. M. Tauris, R. S. Lynch, M. H. van Kerkwijk, M. Kramer, C. Bassa, V. S. Dhillon, T. Driebe *et al.*, A massive pulsar in a compact relativistic binary, Science **340**, 1233232 (2013).

[7] H. T. Cromartie, E. Fonseca, S. M. Ransom, P. B. Demorest, Z. Arzoumanian, H. Blumer, P. R. Brook, M. E. DeCesar, T. Dolch, J. A. Ellis, R. D. Ferdman, E. C. Ferrara, N. Garver-Daniels, P. A. Gentile, M. L. Jones, M. T. Lam, D. R. Lorimer, R. S. Lynch, M. A. McLaughlin, C. Ng *et al.*, Relativistic Shapiro delay measurements of an extremely massive millisecond pulsar, Nat. Astron. **4**, 72 (2020).

[8] B. P. Abbott, R. Abbott, T. D. Abbott, F. Acernese, K. Ackley, C. Adams, T. Adams, P. Addesso, R. X. Adhikari, V. B. Adya *et al.*, GW170817: Observation of Gravitational Waves from a Binary Neutron Star Inspiral, Phys. Rev. Lett. **119**, 161101 (2017).

[9] M. C. Miller, F. K. Lamb, A. J. Dittmann, S. Bogdanov, Z. Arzoumanian, K. C. Gendreau, S. Guillot, A. K. Harding, W. C. G. Ho, J. M. Lattimer, R. M. Ludlam, S. Mahmoodifar, S. M. Morsink, P. S. Ray, T. E. Strohmayer, K. S. Wood, T. Enoto, R. Foster, T. Okajima, G. Prigozhin *et al.*, PSR J0030 + 0451 mass and radius from nicer data and implications for the properties of neutron star matter, Astrophys. J. Lett. **887**, L24 (2019).

[10] T. E. Riley, A. L. Watts, S. Bogdanov, P. S. Ray, R. M. Ludlam, S. Guillot, Z. Arzoumanian, C. L. Baker, A. V. Bilous, D. Chakrabarty, K. C. Gendreau, A. K. Harding, W. C. G. Ho, J. M. Lattimer, S. M. Morsink, and T. E. Strohmayer, A nicer view of PSR J0030+0451: Millisecond pulsar parameter estimation, Astrophys. J. Lett. **887**, L21 (2019).

[11] R. Essick, P. Landry, A. Schwenk, and I. Tews, Detailed examination of astrophysical constraints on the symmetry energy and the neutron skin of ^{208}Pb with minimal modeling assumptions, Phys. Rev. C **104**, 065804 (2021).

[12] B.-A. Li, B.-J. Cai, W.-J. Xie, and N.-B. Zhang, Progress in constraining nuclear symmetry energy using neutron star observables since GW170817, Universe **7**, 182 (2021).

[13] C. Drischler, J. W. Holt, and C. Wellenhofer, Chiral effective field theory and the high-density nuclear equation of state, Annu. Rev. Nucl. Part. Sci. **71**, 403 (2021).

[14] P. Haensel, A. Y. Potekhin, and D. G. Yakovlev, *Neutron Stars 1: Equation of State and Structure* (Springer, New York, USA, 2007), Vol. 326.

[15] J. M. Lattimer, Neutron stars, Gen. Relativ. Gravitation **46**, 1713 (2014).

[16] G. Baym, T. Hatsuda, T. Kojo, P. D. Powell, Y. Song, and T. Takatsuka, From hadrons to quarks in neutron stars: A review, Rep. Prog. Phys. **81**, 056902 (2018).

[17] K. Hebeler, J. M. Lattimer, C. J. Pethick, and A. Schwenk, Constraints on Neutron Star Radii Based on Chiral Effective Field Theory Interactions, Phys. Rev. Lett. **105**, 161102 (2010).

[18] K. Hebeler, J. M. Lattimer, C. J. Pethick, and A. Schwenk, Equation of state and neutron star properties constrained by nuclear physics and observation, Astrophys. J. **773**, 11 (2013).

[19] J. M. Lattimer, The nuclear equation of state and neutron star masses, Annu. Rev. Nucl. Part. Sci. **62**, 485 (2012).

[20] Z. Arzoumanian, A. Brazier, S. Burke-Spolaor, S. Chamberlin, S. Chatterjee, B. Christy, J. M. Cordes, N. J. Cornish, F. Crawford, H. Thankful Cromartie *et al.*, The nanograv 11-year data set: High-precision timing of 45 millisecond pulsars, Astrophys. J., Suppl. Ser. **235**, 37 (2018).

[21] G. Raaijmakers, T. E. Riley, A. L. Watts, S. K. Greif, S. M. Morsink, K. Hebeler, A. Schwenk, T. Hinderer, S. Nissanke, S. Guillot, Z. Arzoumanian, S. Bogdanov, D. Chakrabarty, K. C. Gendreau, W. C. G. Ho, J. M. Lattimer, R. M. Ludlam, and M. T. Wolff, A NICER view of PSR J0030 + 0451: Implications for the dense matter equation of state, Astrophys. J. Lett. **887**, L22 (2019).

[22] J. W. T. Hessels, S. M. Ransom, I. H. Stairs, P. C. C. Freire, V. M. Kaspi, and F. Camilo, A radio pulsar spinning at 716 Hz, Science **311**, 1901 (2006).

[23] C. G. Bassa, Z. Pleunis, J. W. T. Hessels, E. C. Ferrara, R. P. Breton, N. V. Gusinskaia, V. I. Kondratiev, S. Sanidas, L.

Nieder, C. J. Clark *et al.*, Lofar discovery of the fastest-spinning millisecond pulsar in the galactic field, Astrophys. J. Lett. **846**, L20 (2017).
[24] R. W. Romani, D. Kandel, A. V. Filippenko, T. G. Brink, and W. Zheng, PSR J0952-0607: The fastest and heaviest known galactic neutron star, Astrophys. J. Lett. **934**, L17 (2022).
[25] D. Adhikari *et al.*, Precision Determination of the Neutral Weak form Factor of ^{48}Ca, Phys. Rev. Lett. **129**, 042501 (2022).
[26] D. Adhikari, H. Albataineh, D. Androic, K. Aniol, D. S. Armstrong, T. Averett, C. Ayerbe Gayoso, S. Barcus, V. Bellini, R. S. Beminiwattha *et al.*, Accurate Determination of the Neutron Skin Thickness of ^{208}Pb Through Parity-Violation in Electron Scattering, Phys. Rev. Lett. **126**, 172502 (2021).
[27] Z. Zhang and L.-W. Chen, Bayesian inference of the symmetry energy and the neutron skin in ^{48}Ca and ^{208}Pb from CREX and PREX-2, arXiv:2207.03328.
[28] P.-G. Reinhard, X. Roca-Maza, and W. Nazarewicz, Combined Theoretical Analysis of the Parity-Violating Asymmetry for ^{48}Ca and ^{208}Pb, Phys. Rev. Lett. **129**, 232501 (2022).
[29] J. M. Lattimer, Constraints on nuclear symmetry energy parameters, Particles **6**, 30 (2023).
[30] B. T. Reed, F. J. Fattoyev, C. J. Horowitz, and J. Piekarewicz, Implications of PREX-2 on the Equation of State of Neutron-Rich Matter, Phys. Rev. Lett. **126**, 172503 (2021).
[31] P. Danielewicz, R. Lacey, and W. G. Lynch, Determination of the equation of state of dense matter, Science **298**, 1592 (2002).
[32] S. K. Dhiman, R. Kumar, and B. K. Agrawal, Nonrotating and rotating neutron stars in the extended field theoretical model, Phys. Rev. C **76**, 045801 (2007).
[33] R. Kumar, B. K. Agrawal, and Shashi K. Dhiman, Effects of ω meson self-coupling on the properties of finite nuclei and neutron stars, Phys. Rev. C **74**, 034323 (2006).
[34] C. J. Horowitz and J. Piekarewicz, Neutron Star Structure and the Neutron Radius of ^{208}Pb, Phys. Rev. Lett. **86**, 5647 (2001).
[35] H. Müller and B. D. Serot, Relativistic mean-field theory and the high-density nuclear equation of state, Nucl. Phys. A **606**, 508 (1996).
[36] B. K. Pradhan, D. Chatterjee, R. Gandhi, and J. Schaffner-Bielich, Role of vector self-interaction in neutron star properties, Nucl. Phys. A **1030**, 122578 (2023).
[37] F. J. Fattoyev, C. J. Horowitz, J. Piekarewicz, and B. Reed, GW190814: Impact of a 2.6 solar mass neutron star on the nucleonic equations of state, Phys. Rev. C **102**, 065805 (2020).
[38] V. Thakur, R. Kumar, P. Kumar, V. Kumar, B. K. Agrawal, and S. K. Dhiman, Relativistic mean field model parametrizations in the light of GW170817, GW190814, and PSR J0740 + 6620, Phys. Rev. C **106**, 025803 (2022).
[39] R. J. Furnstahl, B. D. Serot, and H.-B. Tang, A chiral effective Lagrangian for nuclei, Nucl. Phys. A **615**, 441 (1997).
[40] T. J. Bürvenich, D. G. Madland, and P.-G. Reinhard, Adjustment studies in self-consistent relativistic mean-field models, Nucl. Phys. A **744**, 92 (2004).
[41] S. Kirkpatrick, Optimization by simulated annealing: Quantitative studies, J. Stat. Phys. **34**, 975 (1984).
[42] J. Dobaczewski, W. Nazarewicz, and P. G. Reinhard, Error estimates of theoretical models: A guide, J. Phys. G **41**, 074001 (2014).
[43] M. Wang, G. Audi, F. G. Kondev, W. J. Huang, S. Naimi, and X. Xu, The AME2016 atomic mass evaluation, Chin. Phys. C **41**, 030003 (2017).
[44] M. Wang, W. J. Huang, F. G. Kondev, G. Audi, and S. Naimi, The AME 2020 atomic mass evaluation (II). Tables, graphs and references, Chin. Phys. C **45**, 030003 (2021).
[45] E. W. Otten, *Treatise on Heavy-Ion Science*, edited by D. A. Bromley (Plenum Press, New York, 1989), Vol. 8, p. 517.
[46] H. De Vries, C. W. De Jager, and C. De Vries, Nuclear charge and magnetization density distribution parameters from elastic electron scattering, Atom. Data Nucl. Data Tabl. **36**, 495 (1987).
[47] P. Ring and P. Schuck, *The Nuclear Many-Body Problem* (Springer Science & Business Media, 1980).
[48] S. Karatzikos, A. V. Afanasjev, G. A. Lalazissis, and P. Ring, The fission barriers in actinides and superheavy nuclei in covariant density functional theory, Phys. Lett. B **689**, 72 (2010).
[49] Siegmund Brandt, *Statistical and Computational Methods in Data Analysis* (Springer, 19970).
[50] G. A. Lalazissis, J. König, and P. Ring, New parametrization for the Lagrangian density of relativistic mean field theory, Phys. Rev. C **55**, 540 (1997).
[51] F. J. Fattoyev and J. Piekarewicz, Accurate calibration of relativistic mean-field models: Correlating observables and providing meaningful theoretical uncertainties, Phys. Rev. C **84**, 064302 (2011).
[52] C. Mondal, B. K. Agrawal, and J. N. De, Constraining the symmetry energy content of nuclear matter from nuclear masses: A covariance analysis, Phys. Rev. C **92**, 024302 (2015).
[53] B.-A. Li and X. Han, Constraining the neutron–proton effective mass splitting using empirical constraints on the density dependence of nuclear symmetry energy around normal density, Phys. Lett. B **727**, 276 (2013).
[54] P.-G. Reinhard, X. Roca-Maza, and W. Nazarewicz, Information Content of the Parity-Violating Asymmetry in ^{208}Pb, Phys. Rev. Lett. **127**, 232501 (2021).
[55] G. Colo, U. Garg, and H. Sagawa, Symmetry energy from the nuclear collective motion: Constraints from dipole, quadrupole, monopole and spin-dipole resonances, Eur. Phys. J. A **50**, 26 (2014).
[56] J. Piekarewicz, Symmetry energy constraints from giant resonances: A relativistic mean-field theory overview, Eur. Phys. J. A **50**, 25 (2014).
[57] J. Zimmerman, Z. Carson, K. Schumacher, A. W. Steiner, and K. Yagi, Measuring nuclear matter parameters with nicer and LIGO/Virgo, arXiv:2002.03210.
[58] William G. Newton and G. Crocombe, Nuclear symmetry energy from neutron skins and pure neutron matter in a Bayesian framework, Phys. Rev. C **103**, 064323 (2021).
[59] J. Xu and P. Papakonstantinou, Bayesian inference of finite-nuclei observables based on the kids model, Phys. Rev. C **105**, 044305 (2022).
[60] H. Gil, P. Papakonstantinou, and C. H. Hyun, Constraints on the curvature of nuclear symmetry energy from recent astronomical data within the kids framework, Int. J. Mod. Phys. E **31**, 2250013 (2022).
[61] B.-A. Li, B.-J. Cai, W.-J. Xie, and N.-B. Zhang, Progress in constraining nuclear symmetry energy using neutron star observables since GW170817, Universe **7**, 2021 (2021).
[62] T.-G. Yue, L.-W. Chen, Z. Zhang, and Y. Zhou, Constraints on the symmetry energy from PREX-II in the multimessenger era, Phys. Rev. Res. **4**, L022054 (2022).

[63] W.-C. Chen and J. Piekarewicz, Searching for isovector signatures in the neutron-rich oxygen and calcium isotopes, Phys. Lett. B **748**, 284 (2015).
[64] W. G. Lynch, M. B. Tsang, Y. Zhang, P. Danielewicz, M. Famiano, Z. Li, and A. W. Steiner, Probing the symmetry energy with heavy ions, Prog. Part. Nucl. Phys. **62**, 427 (2009).
[65] M. B. Tsang, Y. Zhang, P. Danielewicz, M. Famiano, Z. Li, W. G. Lynch, and A. W. Steiner, Constraints on the Density Dependence of the Symmetry Energy, Phys. Rev. Lett. **102**, 122701 (2009).
[66] P. Danielewicz and J. Lee, Symmetry energy II: Isobaric analog states, Nucl. Phys. A **922**, 1 (2014).
[67] A. W. Steiner, J. M. Lattimer, and E. F. Brown, The equation of state from observed masses and radii of neutron stars, Astrophys, J. **722**, 33 (2010).
[68] J. Nättilä, A. W. Steiner, J. J. E. Kajava, V. F. Suleimanov, and J. Poutanen, Equation of state constraints for the cold dense matter inside neutron stars using the cooling tail method, Astron. Astrophys. **591**, A25 (2016).
[69] J. R. Oppenheimer and G. M. Volkoff, On massive neutron cores, Phys. Rev. **55**, 374 (1939).
[70] R. C. Tolman, Static solutions of Einstein's field equations for spheres of fluid, Phys. Rev. **55**, 364 (1939).
[71] G. Baym, C. Pethick, and P. Sutherland, The ground state of matter at high densities: Equation of state and stellar models, Astrophys. J. **170**, 299 (1971).
[72] E. Annala, T. Gorda, A. Kurkela, and A. Vuorinen, Gravitational-Wave Constraints on the Neutron-Star-Matter Equation of State, Phys. Rev. Lett. **120**, 172703 (2018).
[73] T. Hinderer, Tidal love numbers of neutron stars, Astrophys. J. **677**, 1216 (2008).
[74] T. Hinderer, B. D. Lackey, R. N. Lang, and J. S. Read, Tidal deformability of neutron stars with realistic equations of state and their gravitational wave signatures in binary inspiral, Phys. Rev. D **81**, 123016 (2010).
[75] T. Hinderer, Astrophys. J. **697**, 964 (2009).
[76] T. Damour and A. Nagar, Effective one body description of tidal effects in inspiralling compact binaries, Phys. Rev. D **81**, 084016 (2010).
[77] Y. Li, H. Chen, D. Wen, and J. Zhang, Constraining the nuclear symmetry energy and properties of the neutron star from GW170817 by Bayesian analysis, Eur. Phys. J. A **57**, 31 (2021).
[78] B. Biswas, Impact of PREX-II and combined radio/NICER/XMM-Newton's mass–radius measurement of PSR J0740+ 6620 on the dense-matter equation of state, Astrophys. J. **921**, 63 (2021).
[79] I. Legred, K. Chatziioannou, R. Essick, S. Han, P. Landry *et al.*, Impact of the PSR J0740+ 6620 radius constraint on the properties of high-density matter, Phys. Rev. D **104**, 063003 (2021).
[80] F. J. Fattoyev, J. Piekarewicz, and C. J. Horowitz, Neutron Skins and Neutron Stars in the Multimessenger Era, Phys. Rev. Lett. **120**, 172702 (2018).